Available online at www.sciencedirect.com

jmr&t Journal of Materials Research and Technology

journal homepage: www.elsevier.com/locate/jmrt

Original Article

Electronic transport mechanism and defect states for p-InP/i-InGaAs/n-InP photodiodes

Thi Kim Oanh Vu [a,*], *Minh Tien Tran* [a], *Nguyen Xuan Tu* [a], *Nguyen Thi Thanh Bao* [a], *Eun Kyu Kim* [b,**]

[a] *Institute of Physics, Vietnam Academy of Science and Technology, No. 10 Dao Tan, Viet Nam*

[b] *Department of Physics and Research Institute for Natural Sciences, Hanyang University, Seoul 04763, Republic of Korea*

ARTICLE INFO

Article history:
Received 26 April 2022
Accepted 5 June 2022
Available online 12 June 2022

Keywords:
p-InP/i-InGaAs/n-InP photodiode
Defect states
Electronic transport
DLTS
MBE

ABSTRACT

We have studied the defect states and electronic transport mechanisms in the mismatched p-InP/i-InGaAs/n-InP photodiode grown by molecular beam epitaxy (MBE) using deep-level transient spectroscopy (DLTS) and current–voltage (I–V) measurements. Two defect states were observed in the p-InP layer, which could have originated from Zn diffusion, and another one detected in i-InGaAs acted as a dislocation defect. The total defect density of the device estimated by DLTS and space-charge limited current (SCLC) was about 4×10^{13}, which was much lower than the device grown by other methods. I–V measurements pointed out that the leakage current in this photodiode was caused by the existence of defect states and the small conduction band offset. Therefore, to suppress the leakage current in the devices, it is urgent to reduce the trap density and optimize the thickness of the p-InP layer. The study of defect state and electronic transport mechanism in p-InP/i-InGaAs/n-InP PIN diodes could help to develop a strategy to improve the SWIR sensing technology in the future.

© 2022 The Authors. Published by Elsevier B.V. This is an open access article under the CC BY-NC-ND license (http://creativecommons.org/licenses/by-nc-nd/4.0/).

1. Introduction

Recently, there has been a significant increase in interest in the characterization of p-InP/i-InGaAs/n-InP photodetectors due to their applications in chemical sensing and fibre optic communication [1–4]. InP has been used to make the high performance optoelectronic devices in the wavelength range of 1.1–1.6 μm, and the longer detection range can be achieved by mismatching with InGaAs [5,6]. To improve the properties of p-InP/i-InGaAs/n-InP photodetectors, it is very important to obtain a high quality InGaAs epitaxial layer. Some epitaxial techniques such as metal organic chemical vapor deposition (MOCVD) [7], and liquid phase epitaxy (LPE) [8] have enable us to grow devices where the film thickness and fracture of a heterointerface can be precisely controlled. However, molecular beam epitaxy (MBE) is more commonly used than other techniques [9,10] to produce high quality photodetectors, which are important for long-lived optical communication systems.

* Corresponding author.
** Corresponding author.
E-mail addresses: oanhvtk@iop.vast.vn (T.K. Oanh Vu), ek-kim@hanyang.ac.kr (E.K. Kim).

https://doi.org/10.1016/j.jmrt.2022.06.028

2238-7854/© 2022 The Authors. Published by Elsevier B.V. This is an open access article under the CC BY-NC-ND license (http://creativecommons.org/licenses/by-nc-nd/4.0/).

Currently, the extended wavelength of p-InP/i-InGaAs/n-InP detectors suffers from the dark current. The increase of Indium composition above 0.53 usually leads to a relatively large mismatch between the InGaAs layer and the InP layers, resulting in an increase of defect and trap density in the forbidden band gap, which in turn is the cause of dark current [11]. It is also suggested that the high dark current in the photodetectors could be caused by generation-recombination centers associated with dislocations [12]. To successfully realize the dark current mechanism and further avoid the dark current in the photodetector, it is necessary to understand the characterization of defects and traps in the absorption layers. Deep-level transient spectroscopy (DLTS) is a powerful tool to study the defect states in semiconductor devices [13–17]. The method was initially introduced by D.V. Lang [18] in 1974 which used the capacitance of the p–n junction or Schottky barrier as a monitor of the changes in the deep defect state. DLTS is a sensitive, rapid, and easy to analyze technique that can give reliable information on the defect concentration, activation energy, and capture rates of the different traps. Besides, space-charged limited current (SCLC) is another efficient technique to estimate the low concentration of deep-level defects with high accuracy and sensitivity [19]. Nowadays, few articles combine these two methods DLTS and SCLC to deeply understand the defect states in the semiconductor devices.

In this study, we elucidate the electrical characteristics and the defects of p-InP/i-InGaAs/n-InP photodiode grown by MBE. DLTS and SCLC characterizations were performed on the device to obtain the activation energies, capture cross-section, and defect concentrations of all the traps. I–V curves also have been extracted to investigate the sources of leakage current.

2. Experimental methods

The cross-sectional view of the sample for the electrical measurements is shown in Fig. 1(a). The sample was prepared using molecular beam epitaxy (MBE). A 250 nm InP was grown on an n-type InP substrate with a doping concentration of 10^{16} cm^{-3}, and the 200 nm InGaAs layer followed with a doping concentration of 10^{16} cm^{-3}. An n-type InP doped Si top layer with a thickness of 1 μm was grown over the InGaAs layer, followed by 2.5 μm InGaAs. The carrier concentrations of n-type InP and InGaAs were 2×10^{18} cm^{-3} and 10^{16} cm^{-3}, respectively. Finally, the heterostructures of the photodetector was completed with 0.5 μm InP with a doping density of 10^{16} cm^{-3}. Zn was diffused during fabricating the 0.5 μm InP layer. A scanning electron microscope (SEM) image of the p-InP/i-InGaAs/n-InP heterojunction's cross-section with Zn diffusion on the InP layer is displayed in Fig. 1(b). After the structures were grown, Zn/Au/Cr/Au (20 nm/40 nm/20 nm/300 nm) and Ti/Pt/Au (30 nm/70 nm/300 nm) layers were deposited for the Ohmic contacts using a thermal evaporator with a shadow mask.

The internal mode of the HP 4280 A capacitance meter was used to measure the capacitance–voltage and the time-dependent capacitance transient. The capacitance transients by the HP 4280 A C-meter have measured at 64 points with a sampling time of 50 ms. Measurement temperature was varied in the ranges from 100 K to 330 K continuously by using a closed-cycle refrigerator. The I–V characteristic of the PIN diode was conducted under the illumination of 1070 nm, on the film surface.

3. Results and discussions

Figure 2(a) illustrates the typical I–V curves of InP/InGaAs/InP photodiodes at various temperatures from 140 to 300 K. The applied DC bias ranged from −1 V to 1 V. The dark current of the diodes increases sharply with the augmentation of temperature. Under positive bias, more electrons are excited from the bottom contact layer to the top contact layer because of the higher sheet electron density of the bottom contact layer than in the case of negative bias [20]. This creates the asymmetry of the I–V curves presented in Fig. 2(a). It is well-known

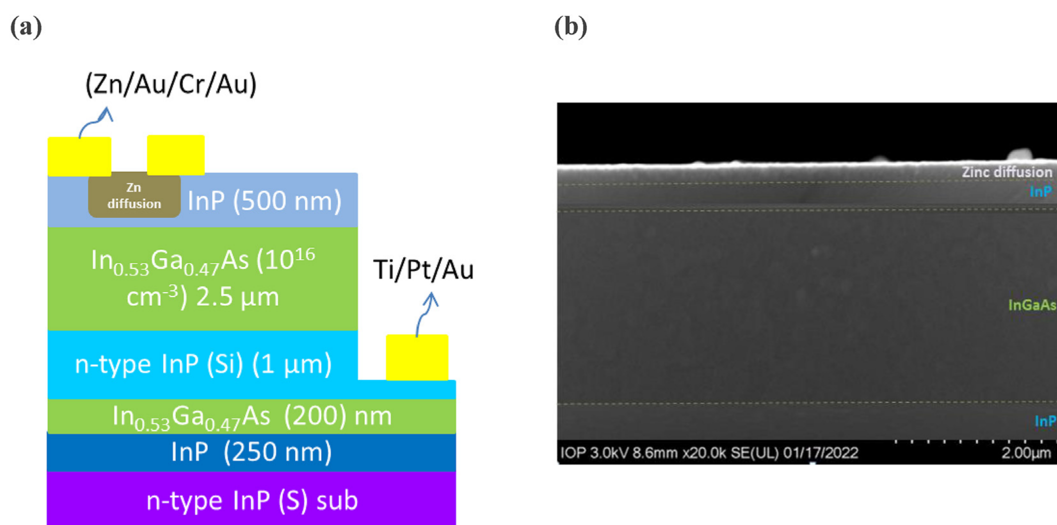

Fig. 1 – (a) The schematic structure of p-InP/i-InGaAs/n-InP photodiode and (b) the SEM image of sample's cross-section.

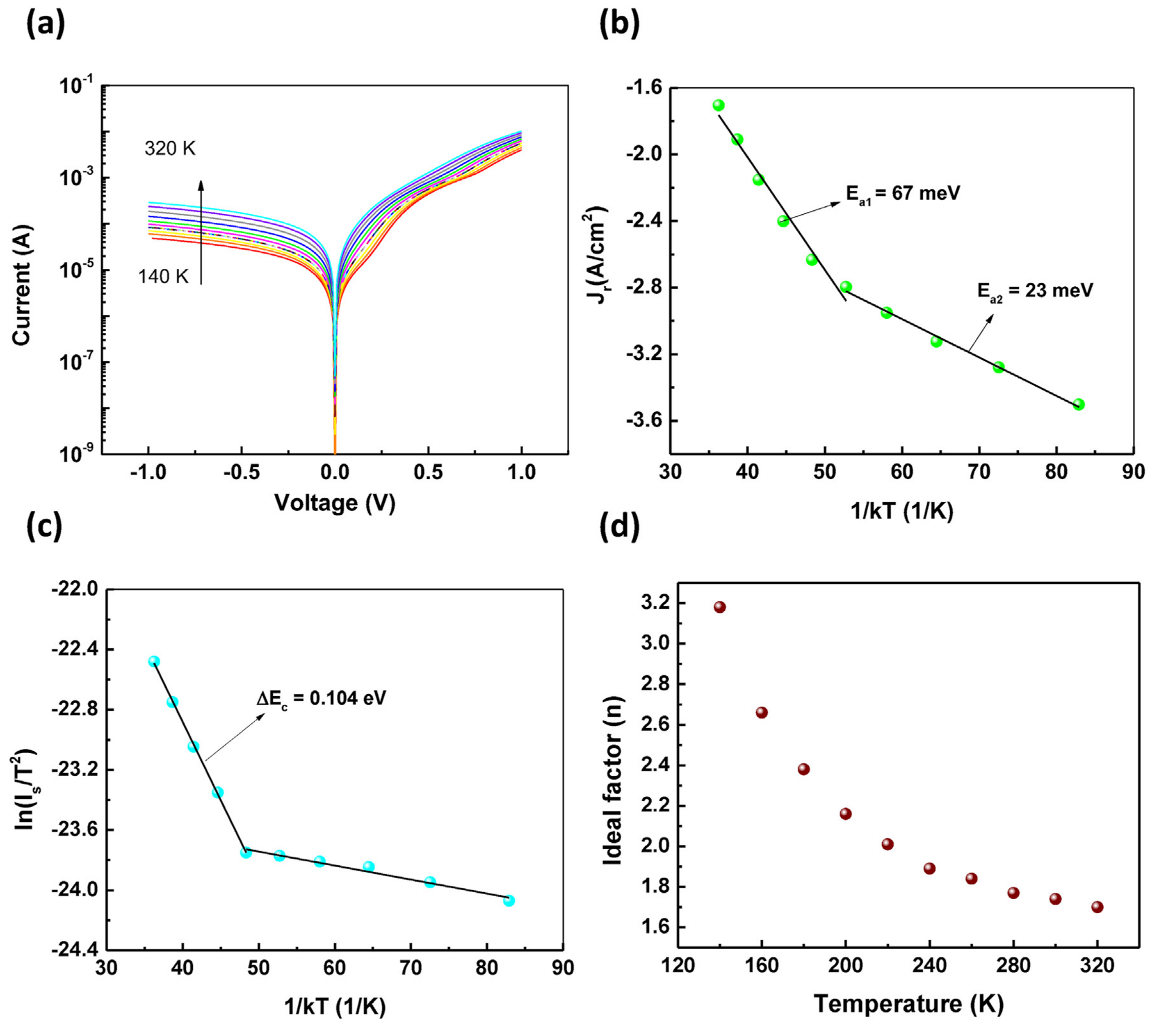

Fig. 2 – (a) The temperature dependence of I–V curves, (b) the dark current density as the function of inverse temperature under bias voltage of −1 V, (c) The plots of ln (I_s/T^2) versus 1/(kT) characteristic under forward bias of 1 V, and (d) ideal impact factor as function of temperature for p-InP/i-InGaAs/n-InP diode.

that the dark current consists of four main mechanisms: diffusions, generation-recombination, defect-assisted tunneling, and band-to-band tunneling [21,22]. To figure out the dominant mechanism of dark current, the dark current density as the function of inverse temperature is given in Fig. 2(b). In this study, we investigate the thermal activation energy (E_a) to identify this dominant mechanism. Theoretically, the relation between the current density J_r, E_a, and temperature T can be expressed as:

$$J_r \sim exp\left(\frac{-E_a}{kT}\right) \quad (1)$$

where k is the Boltzmann constant, T is the temperature in Kelvin and J_r is the concentration of the dark current. The calculated thermal activation energy is about 67 meV at high temperature and about 23 meV at low-temperature range under the operating bias voltage of − 1 V. In fact, the point of 67 meV was discussed in the literature on electron transport in high-performance short-wavelength quantum cascade lasers (E_a = 70 meV) by Laurent Diehl et al. [23]. The leakage current can be attributed to electrons that can easily scatter into the state E_a = 90 meV by thermionic emission. As in the cases of activation energies are too low (E_a = 23 meV), the reason is considered maybe a greater proportion of the collision resulted in the reactions or it means their physical origin might be a diffusion of metal species from Ohmic contacts toward semiconductor layer [24].

In the forward bias region, for the structures of p-InP/i-InGaAs/n-InP photodetector, it is assumed that the relation between the applied forward bias and current of the structures can be expressed as:

$$I = I_s exp\left[\frac{q(V - IR_s)}{nkT}\right]\left[1 - exp\left[\frac{q(V - IR_s)}{nkT}\right]\right] \quad (2)$$

where k is the Boltzmann constant, T is the temperature in Kelvin, V is applied voltage, R_s due to the bulk and contact resistance and n is called ideal factor. I_s is the saturation current given by:

$$I_s = A^* AT^2 exp\left[\frac{-q\Delta E_c}{kT}\right] \quad (3)$$

where q is the electron charge, A*, A, and ΔE_c are the effective Richardson constant, the area of the rectifier contact, and the conduction band offset, respectively. The plots of the ln (I_s/T^2) versus 1/(kT) characteristics for p-InP/i-InGaAs/n-InP photodiode in the temperature range from 140 K to 320 K under a forward voltage of 1 V are shown in Fig. 2(c). It can be seen that ΔE_c values show an unusual behavior that increases with increasing temperature. The variation of band offset splitting is the most important cause of the difference between two material systems in handling optical power. This is because band-offset energy determines the escape times of the charge carrier. According to admittance spectroscopy and photoluminescence, excitation spectroscopy, the ΔE_c for the InGaAs/InP heterostructure is about 0.4 E_g [25] with an energy band gap of $In_{0.53}Ga_{0.47}As$ of 0.75 eV. However, the maximum fit to the ΔE_c data according to equation (3) yields the values of ΔE_c = 104 meV to be consistent with Fig. 2(b), which is lower than 0.4 E_g. These low conduction band offset values cause electrons easily overflow from the photodetector, which increases the leakage current and degrades the optical characteristics. The extracted ideal factor of the device at the different temperatures is presented in Fig. 2(d). It is worth noting that at 220 K, the gradient of the ideal factor changes with the temperature gradient and the ideal factor gradually reduces with increasing temperature. At 320 K, the ideal factor exposes the value of about 1.7 eV, which is nearly close to an ideal diode (n = 1).

A better explanation of the origin of the dark current in the photodiode requires the identification of the defects by C–V and DLTS measurements. The C–V measurements are widely used to evaluate an arbitrary impurity distribution. The carrier concentration at the edge of the depletion region is expressed as:

$$N(W) = \frac{2}{q\varepsilon_s}\left[\frac{1}{d\left(\frac{1}{C^2}\right)/dV}\right] \tag{4}$$

where ε_s the dielectric constant of InP, and W is the depletion width that is extracted from C–V measurement:

$$W = \frac{C}{\varepsilon_s} \tag{5}$$

The carrier profile extracted from the result of the C–V measurement of the InP/InGaAs/InP photodetectors, which was used to find the bias condition for the DLTS measurements, is shown in Fig. 3(a) with the C–V curve inset. The estimated carrier concentration is about 2×10^{16} cm^{-3} and increases slightly with increasing the depletion width of the junction of p-InP/InGaAs transition. This result is higher than the carrier concentration of the p-InGaAs layer which was measured by Hall. The possible reason could be the diffusion of Zn into the InP layer, which leads to the enhancement of carrier concentration. To clearly see the junction width of the PIN photodiode, we show a diagram of this device in the upper part of Fig. 3(b). The upper diagram shows the dimensions and composition of the PIN diode under the reverse bias, where the width of the intrinsic region is W. Under reverse bias, the depletion region was imposed, the total width of the depleted region is W_D, and its fraction in the p-region and n-region is x_p and x_n, respectively. The value of W_D extracted from W and the carrier concentration of InP in the p-region and n-region are as follows:

$$W_D = \left[\frac{2\varepsilon_s(N_a + N_d)(V_{bi} - V)}{qN_aN_d} + W^2\right]^{1/2} \tag{6}$$

here N_a and N_d are the acceptor and donor doping concentration, respectively; V_{bi} is the built-in voltage which was

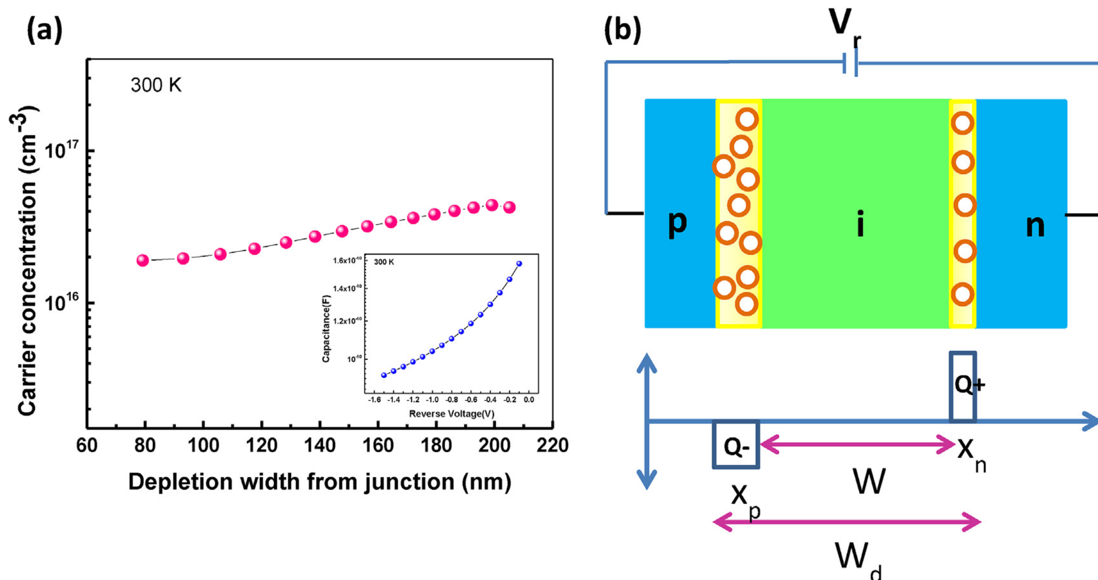

Fig. 3 – (a) The capacitance – voltage characteristics of p-InP/i-InGaAs/n-InP heterostructure measured at 300 K as well as the carrier profiles extracted from the result of the C–V measurements, (b) the dimensions and composition of PIN diode under the reverse bias.

estimated from C–V measurement as illustrated in Fig. S1, and V is the applied bias voltage. Also, x_n and x_p strongly depend on N_a and N_d as:

$$x_n = \frac{N_a(W_D - W)}{N_a + N_d} \tag{7}$$

$$x_p = W_D - W - x_n \tag{8}$$

The value of W_D, x_n, x_p calculated from eqs. (6)–(8) and the reverse bias voltage of −1.5 V are 2845, 0.34, 48.55 nm, respectively. Basing on these values, the position of the defects in p-InP/i-InGaAs/n-InP device can be figured out.

Figure 4(a) and (b) display the DLTS spectra for p-InP/i-InGaAs/n-InP PIN photodiode in the temperature range from 100 to 330 K, emission rate of 0.92 Hz, and applied filling pulse width of 20 ms. In Fig. 3(a), the pulsed bias V_p and the reverse bias or measurement voltage V_m were set to 0 and - 1.5 V, respectively. A broadened DLTS peak was observed, which can be deconvoluted into two distinct peaks H1 and H2 at temperature of 300 and 313 K, respectively. However, when V_p and V_m were changed to 0.5 and 0 V, respectively, the intensity of the two hole peaks H1 and H2 reduced significantly, while, interestingly, a new electron peak E1 appeared. The possible reason for this, as described above, is that under the reverse bias, the depletion width x_p is much higher than x_n, so the source of the two defects H1 and H2 could be originated from the depletion region of the p-InP layer or in the interface state between the p-InP and i-InGaAs layer. The most critical processes are the Zn diffusion through the deposited layers. During the Zinc diffusion, some defects can be formed, which behave like holes trap. This hypothesis, the traps could be concerned with a Zn–related complex in which the point defects due to dislocation movement can be created during diffusion. The stress induced by Zn diffusion at the interface may lead to generate deformation of the InGaAs epilayer and cause lattice mismatch. When the V_p increases to 0.5 V, the depletion region becomes narrower down and the observed electron trap E1 could be attributed to the point defect in InGaAs. To better understand the properties of these defects, the activation energy (E_a), capture cross-section (σ_n), and trap density (N_T) were estimated by plotting the Arrhenius plot (Fig. 4(c)). The activation energy and capture cross-section of

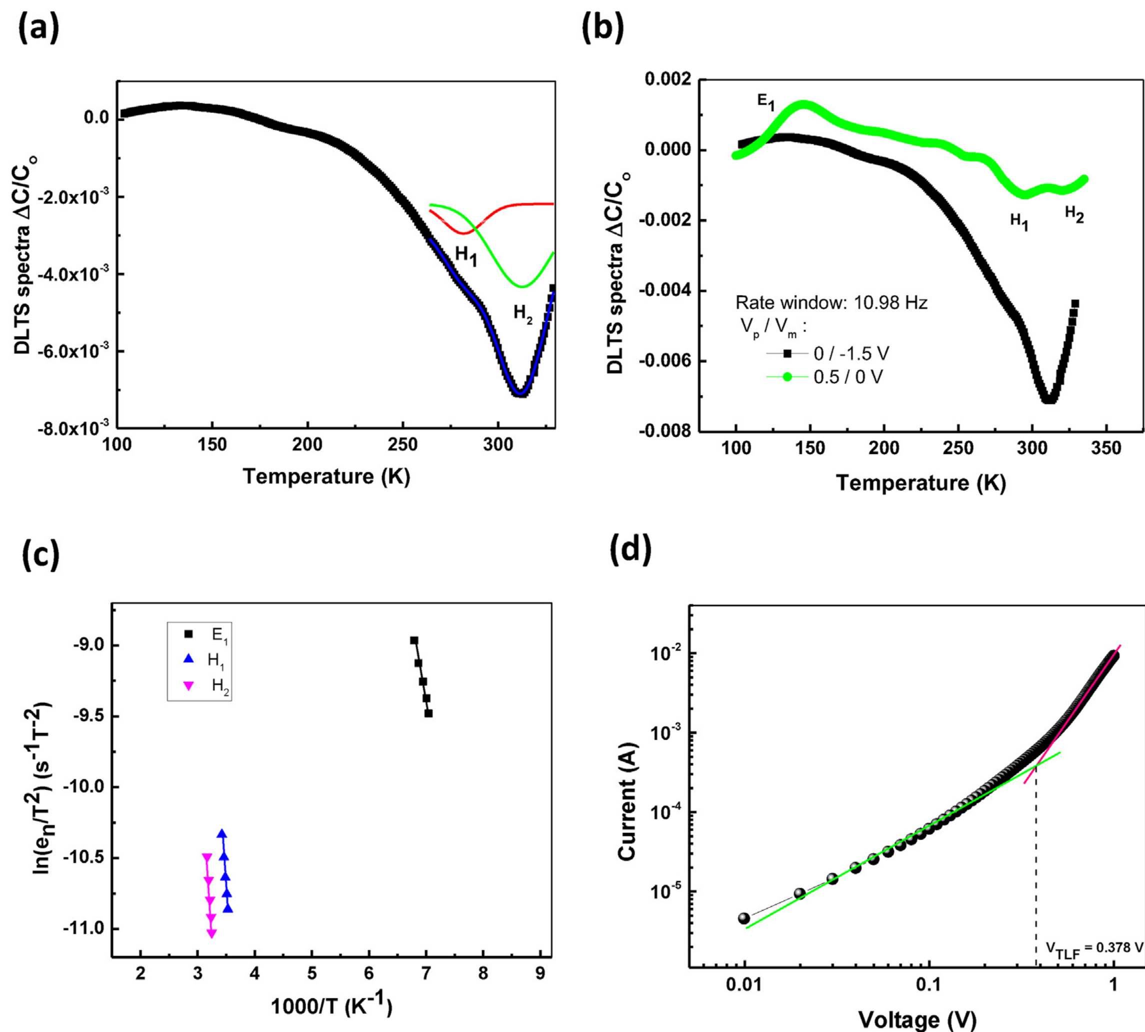

Fig. 4 – (a) DLTS spectra of the heterostructure InP/InGaAs/InP photodiode with the pulse and measure voltages are 0 and -1.5 V, respectively, (b) DLTS spectra with the pulse and measure voltages are 0 and -1.5 V; 0.5 and 0, respectively, (c) Arrhenius plots of the deep traps H_1, H_2, and E_1, and (d) I–V (log–log plot) for the calculation of trap density.

these defect states were extracted from a linear fitting of ln (e_n/T^2) versus 1000/T:

$$\ln\left(\frac{e_n}{T^2}\right)=\ln\left(\frac{\sqrt{6}\pi 1.5k^2 m_h^* \sigma_n}{h^3}\right)+\left(\frac{-\Delta E_a}{1000k}\right)\frac{1000}{T} \quad (9)$$

where e_n is the emission rate, T is the absolute temperature, k Boltzmann's constant, m* is electron effective mass or hole effective mass, and h is Plank's constant.

Base on the carrier concentrations (N_D) extracted from C–V data and DLTS measurement, trap concentrations can be evaluated as follows:

$$N_T = 2N_D\frac{\Delta C(t)}{C(\infty)} \quad (10)$$

From the calculations, the two-hole traps H_1 and H_2 are located at about 0.43 and 0.57 eV above the valence band (E_v) with σ_n of 8.60 × 10^{-18} and 3.11 × 10^{-16} cm^2, respectively. Electron trap E_1 is positioned at 0.28 eV below the conduction band and traps a cross-section of 1.14 × 10^{-12} cm^2. The low cross-section of H1 and H2 indicates that these two defects are point defects in the p-InP layer, while the higher cross-section value of E3 may be caused by the dislocation defect in the InGaAs layer. The values of activation energy in the samples were very similar to the defects (H1 and H2) measured by Du. et al. [26]. The H_2 defect is the dominant defect with a defect density of about 1.38 × 10^{13} cm^{-3}. Meanwhile, the H_1 trap with a relatively low DLTS signal has a concentration of 8.0 × 10^{12}. These low trap densities are comparable to the InP/InGaAs/InP heterostructures grown by MOCVD mentioned in a previous publication [16]. Considering it, we suggest that the InP/InGaAs/InP heterostructures grown by MBE offer more advantages than those grown by MOCVD in the fabrication of high-performance infrared photodetectors. Another effective method for calculating the defect concentration in a device is space-charge

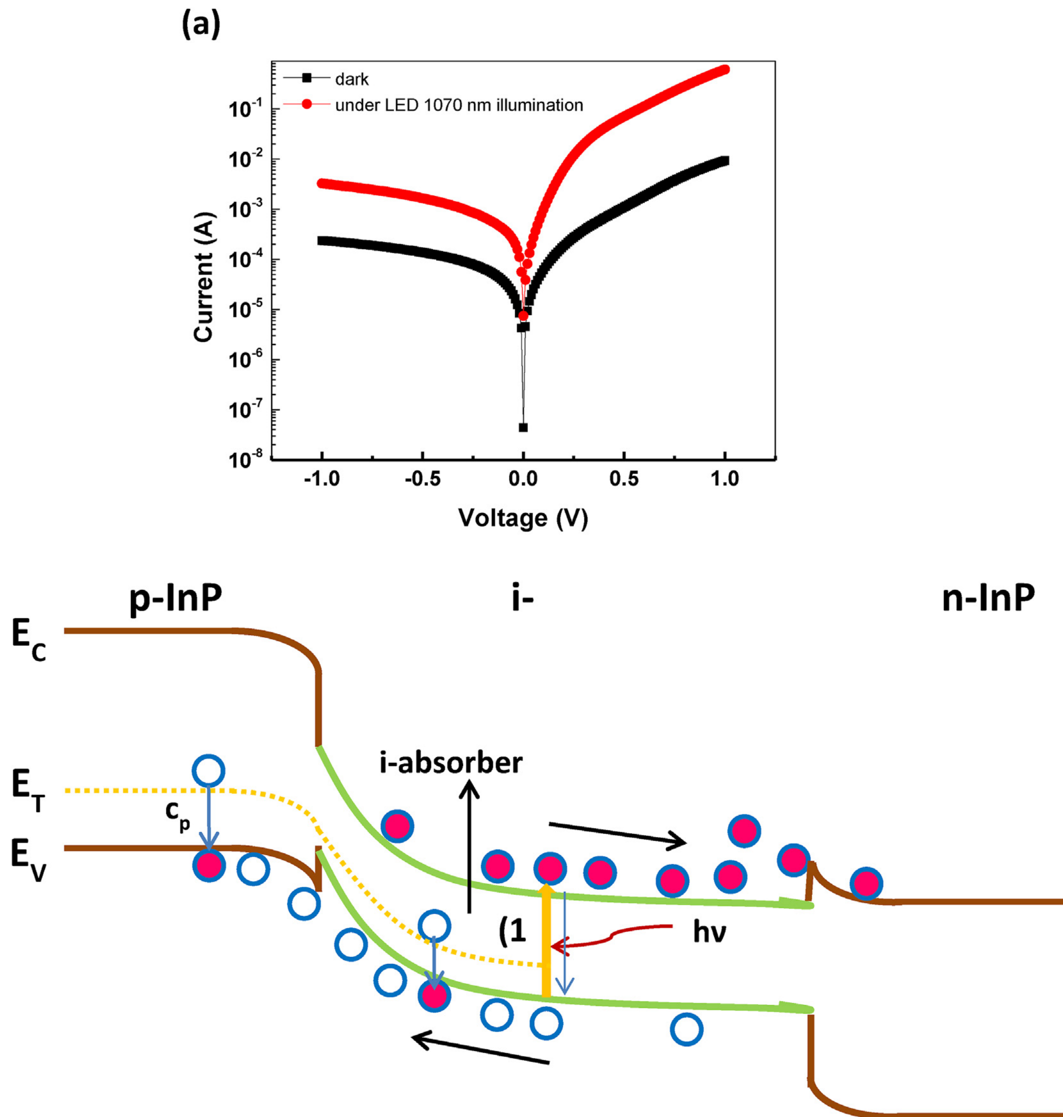

Fig. 5 – (a) Current–voltage characteristics for sample A and B with and without illumination of 1070 nm-LED and (b) carrier transport mechanism in p-InP/i-InGaAs/n-InP photodiode.

limited current (SCLC) technology. The trap density n_t is extracted from the trap-filled limited voltage V_{TFL} as follows:

$$n_t = \frac{2\varepsilon\varepsilon_0.V_{TFL}}{(eL^2)} \quad (11)$$

$$\varepsilon = \frac{C_g.L}{\varepsilon_0 A} \quad (12)$$

Herein ε is dielectric constant, ε_0 is vacuum permittivity, elementary charge e, thickness of the InP layer, geometrical capacitance of the perovskite layer C_g, and active area A. The trap-filled limit voltage V_{TFL} of sample displayed in Fig. 4(c) is 0.378 V with corresponding extracted trap density is about 4×10^{13} cm^{-3}, and it is almost consistent with the total density of defects estimated by DLTS.

To confirm the optoelectronic properties of the devices, we performed I–V measurements in the dark and LED illumination ($\lambda = 1070$ nm) as shown in Fig. 5(a). The ratio of photo/dark current in sample B at a reverse voltage of 1 V is 13.9, indicating that this photodiode detects well under infrared illumination. The mechanism of this detection process and the carrier transport of the p-InP/i-InGaAs/n-InP diode are presented in Fig. 5(b). Process (1) illustrates the electron–hole generation the recombination process when light is illuminated and turned off. The presence of defects in the device would trap the generated holes when the device absorbs the light, resulting in degradation of the photocurrent. In addition, these defects could also trap the recombination carriers when the light was turned off, that leads to a slowdown of the response speed. Therefore, well-control defects in the p-InP/i-InGaAs/n-InP diode play an important role in improving the performance of this device. With a bias voltage of −1 V, at 300 K (room temperature), the calculated conduction band offset (ΔE_C) of the sample is 0.56 V. The low values of conduction band offset cause electrons to easily overflow from the photodetector, which increases the leakage current and degrades the optical characteristics. As reported by Zhiwei et al., the interface defects bring more extra valence band energy (or a decrease in conduction band energy) which can increase the recombination rate, leading to an increase in dark current [27]. Therefore, the optimization of the thickness of the p-InP layer also plays a significant role in the fabrication of InP/InGaAs/InP heterostructures and the production of the promising photodiodes.

4. Conclusions

In conclusion, we fabricated the p-InP/i-InGaAs/n-InP photodiode by MBE. The defect state in photodiode is conducted by DLTS and SCLS method, and two hole traps with activation energy of $E_V + 0.43$ and $E_V + 0.56$ eV were observed in p-InP layer. Zn diffusion was attributed to the existence of these hole traps in the device. Besides, one electron trap E1 was detected, which could be originated from InGaAs layer or p-InP/i-InGaAs interface. The temperature depended I–V curves demonstrated that the leakage current could be attributed to electrons can easily scatter into the state $E_a = 90$ meV by thermionic emission. It is summarized that the excess of defects in p-InP/i-InGaAs/n-InP could degrade the quality of device, so well studying the carrier transportation and the defect states in device are helpful to optimize the photodiode's performance.

Declaration of Competing Interest

The authors declare that they have no known competing financial interests or personal relationships that could have appeared to influence the work reported in this paper.

Acknowledgements

This research was supported by the excellent research team development program grant funded by Vietnam Academy of Science and Technology (VAST) (NCXS 02.05/22–23), and in part supported by National Research Foundation of Korea (NRF) grant funded by the Korean government (MSIT) (NRF-2020R1A4A4078674).

REFERENCES

[1] Smirnov KJ, Medzakovskiy VI, Davydov VV, Vysoczky MG, Glagolev SF. J Phys Conf 2017;917:62019.
[2] Li X, Zhang J, Yue C, Tang X, Gao Z, Jiang Y, et al. Sci Rep 2022;12:7681.
[3] Huang Y-H, Yang C-C, Peng TC, Cheng F-Y, Wu M-C, Tsai Y-T, et al. IEEE Photon Technol Lett 2007;19:5.
[4] Chang S-H, Fang Y-K, Ting S-F, Chen S-F, Lin C-Y, et al. Sens Actuators, A 2007;133:8.
[5] Gilles C, Orbe LJ, Guzma RC, Maisons G, Carras M. Opt Express 2015;23(16):20288–96.
[6] He W, Shao X, Ma Y, Gu Y, Li T, Yang B, et al. AIP Adv 2020;10:65233.
[7] Rybalchenko DV, Mintairov SA, Salii RA, Shavarts MZ, Timoshina N Kh, Kalyuzhnyy NA. Physics of Semiconductor Devices 2017;51:93–9.
[8] Mizuta Ogura M, Onaka K, Kukimoto H. Jpn J Appl Phys 1983;22:1502.
[9] Jasik A, Wnuk A, Gaca J, Wójcik M, Wójcik-Jedlińska A, Muszalski J, et al. J Cryst Growth 2009;311:4423–32.
[10] Feng G, Oe K, Yoshimoto M. J Cryst Growth 2007;301–302:121–4.
[11] Ji X, Liu B, Xu Y, Tang H, Li X, Gong H, et al. J Appl Phys 2013;114(22):224502.
[12] Hoogeveen R, Vander R, Goede A. Infrared Phys Technol 2001;42:1.
[13] Hong W-P, Caneau C, Hayes JR, Bhat R, Chang GK, Nguyen C, et al. J Appl Phys 1991;70(1):502.
[14] Trommer R, Albrecht H. Jpn J Appl Phys 1983;22:6.
[15] Kowalczyk A, Ornoch L, Muszalski J, Kaniewski J, Bak-Misiuk J. Opt Appl 2005;35:457.
[16] Vu TKO, Lee KS, Lee SJ, Kim EK. J Nanosci Nanotechnol 2018;18(9):6239–43.
[17] Vu TKO, Cho I-W, Oh J, Lee DU, Ryu M-Y, Kim EK. J Colloid Interface Sci 2021;590:19–27.
[18] Lang DV. J Appl Phys 1974;45:3023.
[19] Duijinstee EA, Ball JM, Corre VML, Koster LJA, Snaith HJ, Lim J. ACS Energy Lett 2020;5(2):376–84.

[20] Guoqing M, Zhang T, Zhang Z, Jin Y. CrystEngComm 2013;15(42):8461.
[21] Chen B, Yuan J, Holmes AL. Opt Quant Electron 2013;45(3):271–7.
[22] Hoffman D, Nguyen BM, Delaunay PY, Hood A, Razeghi M, Pellegrino J. Appl Phys Lett 2007;91(14):85316.
[23] Christian P, Diehl L, Lyakh A, Wang QJ, Maulini R, Tsekoun A, et al. Opt Express 2010;18(2):746.
[24] Xudong J, Itzler MA, Rafael B-M, Slomkowski K. Advanced Photon Counting Techniques II 2007; 6771:67710S.
[25] Kim K-B, Shin D-S. J Opt Soc Korea 2007;11(3):133–7.
[26] Du AY, Li MF, Chong TC, Teo KL, Lau WS. Appl Phys Lett 1996;69:2849.
[27] Zhang Z, Miao G, Song H, Li D, Jang H, Li Z, et al. Appl Phys A 2017;123:219.